Tunnelling and Underground Space Technology 95 (2020) 103138

Contents lists available at ScienceDirect

Tunnelling and Underground Space Technology

journal homepage: www.elsevier.com/locate/tust

Stability of plane strain tunnel headings in soils with tensile strength cut-off

T.Z. Li, X.L. Yang*

School of Civil Engineering, Central South University, Hunan 410075, China

ARTICLE INFO

Keywords:
Critical face pressure
Plane strain tunnel headings
Modified failure criterion
Tensile strength cut-off

ABSTRACT

This paper focuses on stability analysis of plane strain tunnel headings in soils governed by the modified Mohr-Coulomb failure criterion. In terms of a very small or even zero tensile strength of soils, the tensile strength cut-off is introduced to modify the classical Mohr-Coulomb failure criterion which allows a nonlinear strength envelope of soils in tensile regime. An improved rotational failure mechanism of tunnel face is constructed to search the portion that is subjected to tensile stress along the whole failure block. It is discovered that the face pressure is the most critical when the tensile stress only appears at the top of the failure block. The numerical results obtained by the proposed approach are compared with those without tensile strength cut-off to highlight its influence on tunnel face stability. The finite difference method of FLAC3D is employed to further validate the proposed approach. The variations of cohesion, internal friction angle and unit weight of soils as well as the dimensionless coefficient ξ are investigated using the proposed approach to gain some insight into the improved failure mechanism. The elementary energy analysis is performed by dividing the failure block into numerous infinitesimal elements with respect to the rotation angle to give some extended discussions. It is shown that the top portion of the failure block that plays a role of anti-sliding is cut away due to the tensile strength cut-off, which eventually yields the critical face pressure. Conclusively, the proposed approach is an improved method for the stability analysis of plane strain tunnel headings in soils with tensile strength cut-off.

1. Introduction

It is of great importance to assess the face stability of tunnel headings in unstable media in terms of the fact that tunnel collapses often have their origin in stability problems at the face (Dias and Kastner, 2013; Fraldi and Guarracino, 2011; Ukritchon and Keawsawasvong, 2017; Keawsawasvong and Ukritchon, 2017). With the development of modern tunneling technology, the closed-face tunneling boring machine (TBM) is increasingly used to retain the face stability by providing a continuous face pressure to compensate the earth pressure. Under this circumstance, the critical face pressure, namely the minimum pressure to prevent tunnel collapse, becomes one of the main topics in practical tunnel design. For this purpose, numerous researchers have been devoted to this problem and proposed several approaches to calculate the critical face pressure with the help of numerical simulations, laboratory tests or theoretical analysis (Ibrahim et al., 2015; Ukritchon et al., 2017a, 2017b; Pan and Dias, 2017, 2018; Zingg and Anagnostou, 2018).

As an efficient tool to perform theoretical analysis, the kinematical approach of limit analysis has been widely employed to handle the stability problems of geotechnical structures since it was firstly proposed by Drucker and Prager (1952). In 1975, Chen (1975) published his monograph '*Limit Analysis and Soil Plasticity*' and systematically introduced the limit analysis method and its application in resolving the problems of slope stability, bearing capacity of foundations and so on. An early study to extend this method into tunnel face stability assessment can be found in Leca and Dormieux (1990). In this literature, the upper and lower bound solutions of face pressure for a shallow-buried tunnel driven in frictional media were investigated based on the translational failure mechanism. Mollon et al. (2009) constructed a three-dimensional (3D) failure mechanism to evaluate the stability of a shielded tunnel face by making use of the idea of multi-block mechanisms suggested by Soubra (1999). Michalowski and Drescher (2009) proposed a class of admissible rotational failure mechanisms to assess the stability of slopes and excavations. The velocity field is built based on the assumption that the rigid failure block slides and rotates around the same center. The new achievements about tunnel face stability evaluations can be found from Pan and Dias (2017) who extended the advanced 3D rotational collapse mechanism proposed by Mollon et al. (2011) to generate a failure mechanism for a non-circular tunnel face using the spatial discretization technique. Although the underground excavation stability is essentially a 3D

* Corresponding author.
E-mail address: yangky@aliyun.com (X.L. Yang).

https://doi.org/10.1016/j.tust.2019.103138
Received 1 April 2019; Received in revised form 14 September 2019; Accepted 4 October 2019
Available online 15 October 2019
0886-7798/

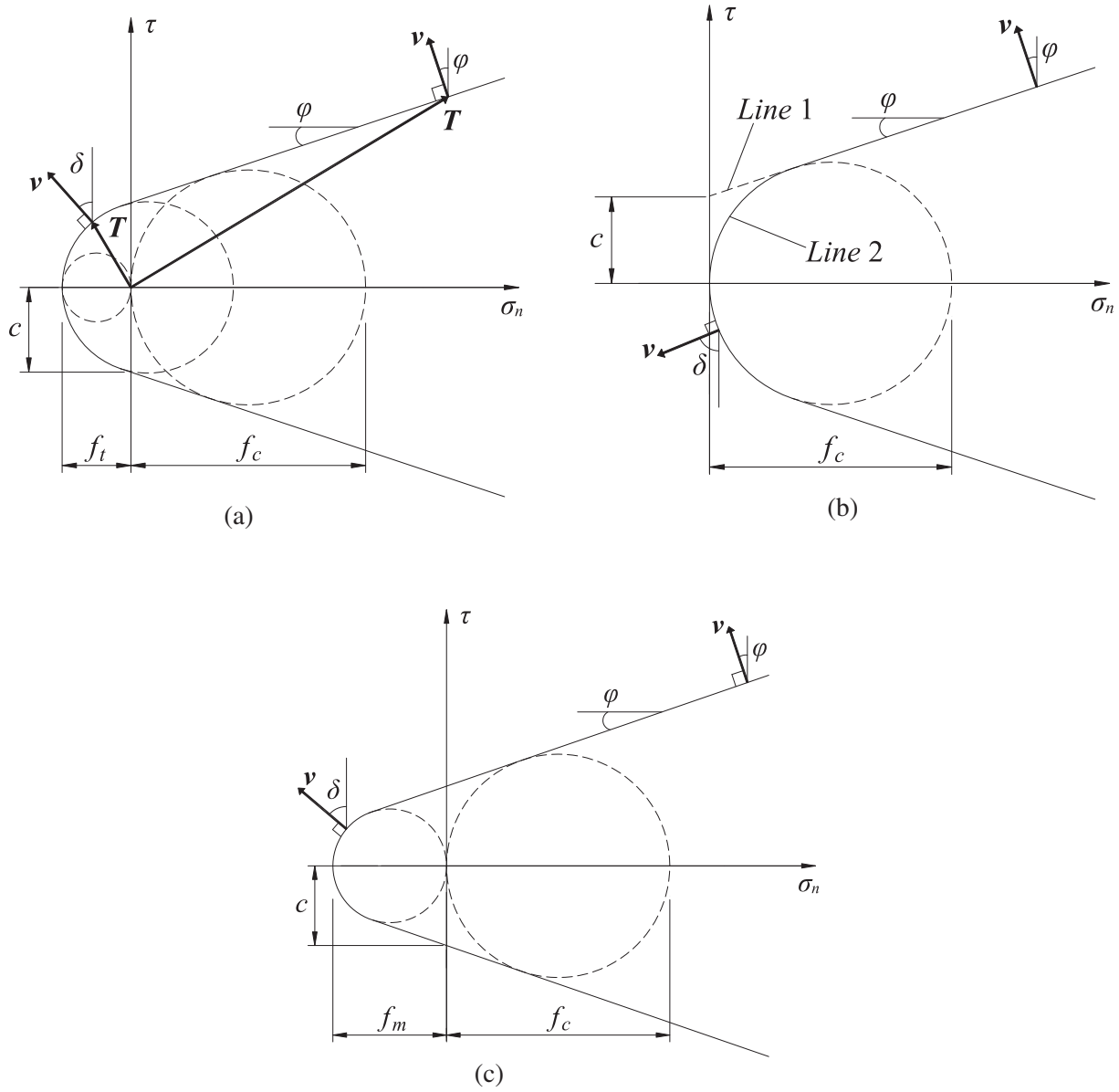

Fig. 1. Strength envelope of Mohr-Coulomb soils with tension cut-off (a) partial tension cut-off (b) full tension cut-off (c) minimum tension cut-off.

problem, it sometimes can be simply represented by a plane strain model. A plane strain tunnel heading can be interesting for a long-wall mining operation or for any flat wall in an underground excavation. Augarde et al. (2003) presented an idealized plane strain heading model for face stability analysis in undrained soil condition. Huang et al. (2020) investigates the stability of existing shield tunnel induced by an adjacent excavation using upper-bound limit analysis method. Ukritchon and Keawsawasvong (2019a, 2019b) performed stability analysis of plane strain tunnel headings in Hoek-Brown rock masses and non-uniform clays using lower bound finite element limit analysis method. All these works help to theoretically interpret the instability behaviors of slopes or tunnel faces.

However, the abovementioned studies fail to recognize that the stress state probably has influence on the failure mechanism, especially for tunnels driven in soils that follow Mohr-Coulomb failure criterion. Researchers often use the classical Mohr-Coulomb failure criterion to describe the strength of soils in regardless of the fact that the strength of soils in tensile regime is remarkably reduced, or even is taken as zero. To address this issue, Paul (1961) gave a plan to limit the tensile strength by using three mutually perpendicular planes to cut the Mohr-Coulomb yield surface in the principle stress space. In the framework of limit analysis method, Michalowsk (1985) adopted the modified Mohr-Coulomb yield condition with a small tension cut-off to characterize the rock failure. Recently, Michalowsk (2017a, 2017b) investigated the stability of soil slopes in which the tensile strength cut-off was taken into account to modify the failure mechanism. Their works give an idea to exclude the actually non-existent tensile strength of geomaterials.

The researches about the effect of tensile strength cut-off on underground excavations are not common in literature. There exist some difficulties in undertaking this study. Firstly, it has been suggested by Duncan and Wright (2005) that either a tension crack or a modified failure envelope should be utilized if the tensile stress can be expected in the theoretical analysis, but only the latter one can be employed in tunnel excavation. Secondly, the face stability assessment is usually performed by postulating a kinematically admissible failure mechanism, but it remains a problem to determine which parts of the pre-postulated failure mechanism are affected by tensile stress. Michalowski (2017), Park and Michalowski (2017) suggested that the tensile stress was more likely to be developed near the top of a slope since a steep failure surface was usually observed at the upper end of

the failure block in practical engineering. Huang et al.(2020) analyzed the stability of a shield tunnel induced by an adjacent excavation. In their study, it was assumed that only the top of the failure mechanism was affected by tensile stress without further explanations. In reality, it does not seem very convincing to directly determine which part of the failure block is in tensile regime for underground excavations.

This paper aims to present a novel procedure to calculate the face pressure of a tunnel in soils governed by the modified Mohr-Coulomb failure criterion. A reduced tensile strength is introduced to modify the failure criterion which leads to a nonlinear strength envelope of soils in tensile regime. The rotational failure mechanism is adopted to characterize the tunnel face failure under the plane strain condition for cohesive-frictional soils (Senent et al. 2013; Smith 2015). The portion of the failure block of tunnel face in tensile regime is determined by the optimization program. The critical face pressures are calculated using the proposed approach and compared with those given by the conventional method to discuss the influence of tensile strength cut-off on tunnel face stability. A plane strain model of FLAC3D is constructed to further validate the proposed approach. The extended discussions are given to figure out how the tensile strength cut-off affects tunnel headings.

2. Tensile strength cut-off

The tensile strength cut-off in soils has attracted little attention in the stability assessment of underground excavations. In most cases, the strength of soils is typically characterized by linear Mohr-Coulomb failure criterion which is usually derived from soil tests in the compressive regime and extrapolation in the tensile regime. As a matter of fact, the uniaxial tensile tests of soils indicate that the strength of soils in the tensile regime does not obey the classical Mohr-Coulomb failure criterion, but is reduced or even taken as zero. It necessitates a modification to the linear strength envelope in the tensile regime to give a better description of the failure behavior of soils that are subjected to tensile stress. To handle this problem, Paul (1961) introduced an efficient strategy to limit the tensile strength using the concept of tension cut-off proposed by Drucker and Prager (1952). The transformation from the principal stress space to τ-σ_n space (τ and σ_n respectively represent the shear stress and normal stress) is quite intricate according to Paul (1961). Several scholars have given an in-depth account of this process, so it is not repeated here. More details can be obtained by referring to Michalowski (2017).

In the framework of limit analysis, the most immediate influence of the tensile strength cut-off can be found in the calculation of internal energy dissipation. As shown in Fig. 1, c and φ refer to the cohesion and internal fraction angle of soils respectively; $\boldsymbol{T}$ is a vector representing the traction on the failure surface in the physical space; $\boldsymbol{v}$ is the velocity vector on the failure surface whose direction is determined by the associated flow rule; δ is the dilatancy angle described by the nonlinear portion of the strength envelope; f_c and f_t respectively denote the uniaxial compressive strength and reduced uniaxial tensile strength. As a result, the internal energy dissipation rate per unit area along the velocity discontinuity whose stress state is defined by the nonlinear portion of the modified Mohr-Coulomb yield condition can be readily calculated as a dot product of the traction vector $\boldsymbol{T}$ and the velocity vector $\boldsymbol{v}$ (Michalowski 2017; Park and Michalowski 2017), namely

$$P_d' = |v|\left(f_c\frac{1-\sin\delta}{2} + f_t\frac{\sin\delta-\sin\varphi}{1-\sin\varphi}\right) \tag{1}$$

where $|\boldsymbol{v}|$ is the magnitude of velocity vector.

According to the classical Mohr-Coulomb function, the uniaxial compressive and tensile strengths, denoted as f_c and f_m respectively, can be expressed as

$$\begin{cases} f_c = \frac{2c\cos\varphi}{1-\sin\varphi} \\ f_m = \frac{2c\cos\varphi}{1+\sin\varphi} \end{cases} \tag{2}$$

For ease of comparison with the classical Mohr-Coulomb failure criterion, the reduced tensile strength f_t is denoted in the form of f_m, namely $f_t = \xi f_m$. So Eq. (1) can be rewritten as

$$P_d' = c\ |v|\left(\cos\varphi\frac{1-\sin\delta}{1-\sin\varphi} + 2\xi\frac{\sin\delta-\sin\varphi}{\cos\varphi}\right) \tag{3}$$

The coefficient ξ ranges from 0 to 1. $\xi = 0$ represents a full tension cut-off with zero tensile strength as shown in Fig. 1b while $\xi = 1$ represents a minimum tension cut-off with $f_t = f_m$ as shown in Fig. 1c. So it is called partial tension cut-off when $0 < \xi < 1$ which corresponds to Fig. 1a. When δ is constantly equal to φ, the internal energy dissipation is degraded to the traditional case without tension cut-off. It can be inferred from Fig. 1 that the range of δ is from φ to 90°. In numerical modelling, there is a classical tension cut-off for Mohr-Coulomb criterion by keeping the full curve in the region where σ_n is greater than 0, such as the Line 1 in Fig. 1b. It can be observed that the shear strength does not transition smoothly to 0, but suddenly changes to 0 when the normal stress is zero. In fact, this case is just a special form of partial tension cut-off.

3. Tunnel face pressure with tensile strength cut-off

3.1. Problem statement

The critical face pressure is an important indicator for face stability assessment of underground headings. It is essential to prevent the tunnel collapse with the minimum economic consumption (Ukritchon and Keawsawasvong, 2019c; Zhang et al., 2019a). Conventional approaches focusing on face pressure calculation prefer to use the classical Mohr-Coulomb failure criterion to construct the failure mechanism ignoring the soils in tensile regime disobeying such a yield condition (Yang and Zhang, 2019; Zhang and Yang, 2019). One major reason is that the tunnels are excavated underground and in most cases, the soil deformation is generated under the influence of compressive stress. The tensile stress probably occurs along the failure surface, but it is difficult to find out which portion of the failure block is affected by tensile stress. In reality, the limit analysis method requires a pre-postulated failure mechanism to build a kinematically admissible velocity field. Therefore, the portion of the failure mechanism that is in tensile regime should also be pre-determined and then the influence of tensile strength cut-off can be taken into account. In this paper, the tunnel face pressure is investigated based on an improved rotational failure mechanism whose upper and lower boundaries are defined by the log-spiral curves in compressive regime and the 'variable-angle log-spiral' curves in tensile regime (Michalowski, 2017; Zhang et al., 2019b). Unlike Li and Yang (2019) where the failure block in tensile regime is limited to the top, this paper developed a novel optimization procedure to numerically determine which portion of the failure mechanism is affected by tensile stress.

As shown in Fig. 2, the failure block is outlined by six key nodes of $ACDE'D'B$. The boundaries of CD and BD' are log-spiral curves. DE' and $D'E'$ are curves determined by the dilatancy angle δ and AC is a curve depending on the dilatancy angle κ. We call them as variable-angle log-spiral curves as suggested by Michalowski (2017). The rigid failure block slides and rotates around the rotation center O with an angular velocity ω. The dilatancy angles δ and κ vary with rotation angle θ with the maximum values δ_m and κ_n at the points E' and A respectively. Notice that δ and κ should continuously change to φ at points C, D and D' to assure the failure surface to be smooth. As suggested by Michalowski (2017), the linear variation of δ or κ as a function of the rotation angle θ can obtain the best estimation of stability of tunnel

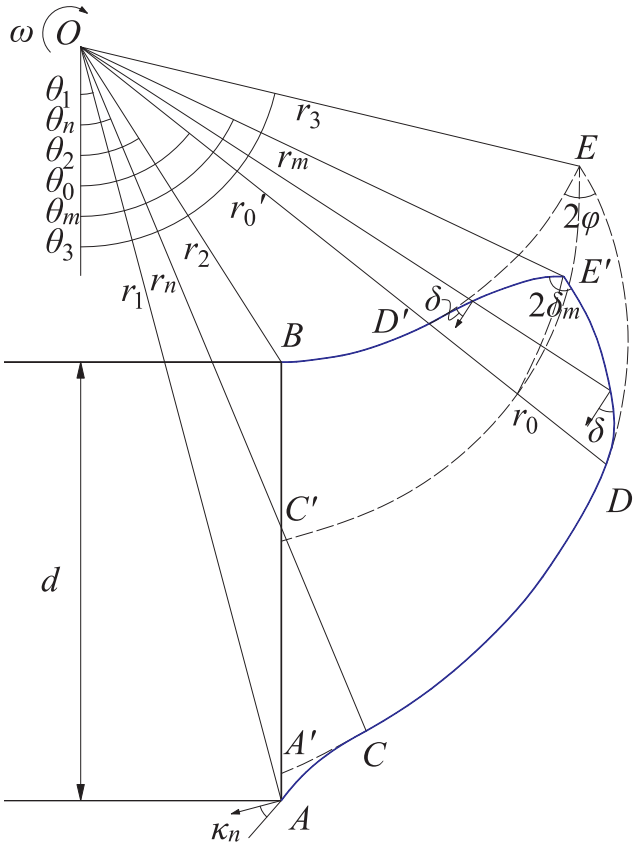

Fig. 2. An improved rotational failure mechanism of tunnel face with tensile strength cut-off.

face. So δ and κ can be expressed as

$$\begin{cases}\delta(\theta)=\frac{\delta_m-\varphi}{\theta_m-\theta_0}(\theta-\theta_0)+\varphi\\ \kappa(\theta)=\frac{\kappa_n-\varphi}{\theta_n-\theta_1}(\theta_n-\theta)+\varphi\end{cases} \tag{4}$$

where θ_0, θ_m, θ_n represent the rotation angles of *OD*, *OE′*, *OC* respectively. The rest parameters listed in Fig. 2 are interpreted as follows. θ_1, θ_2, θ_3 refer to the rotation angles of *OA*, *OB*, *OE* where *E* is the top of the failure block without tensile strength cut-off. *A′* is the intersection of *AB* and the extended line of log-spiral curve *DC*. *C′* is the intersection of *AB* and *OC*. *r* denotes the rotation radius, and the superscripts and subscripts are used to distinguish different points on the failure surface. *d* is the tunnel diameter. As the internal friction angle is necessary for building the kinematically admissible velocity filed, this failure mechanism is only proposed for cohesive-frictional soils or purely frictional soils. In addition, the associated flow rule is assumed for the proposed failure mechanism which leads to an excessive volumetric deformation in soils. This assumption is probably inconsistent with the facts, but necessary. It is because this failure mechanism is generated within the framework of limit analysis where the associated flow rule serves as a basic tool to build the velocity filed. In fact, real soils usually obey the non-associated flow rule since the dilatancy angle of soils is always smaller than the internal friction angle. In contrast, considering the non-associated flow rule can result in a more conservative estimation of critical support pressure.

3.2. Work rate calculation

In order to calculate the critical pressure against tunnel face, the work rate equation is obtained by equating the external work rate to the internal energy dissipation rate according to the proposed failure mechanism. For the variable-angle log-spiral curves of the failure surface, the infinitesimal elements along *AC*, *DE′* and *D′E′* are presented in Fig. 3, resulting in

$$\begin{cases}dr=-r\tan\kappa(\theta)d\theta\\ dr=\mp r\tan\delta(\theta)d\theta\end{cases} \tag{5}$$

then

$$\begin{cases}\int_{r_1}^{r}\frac{dr}{r}=-\int_{\theta_1}^{\theta}\tan\kappa(\theta)d\theta & :AC\ Section\\ \int_{r_0}^{r}\frac{dr}{r}=-\int_{\theta_0}^{\theta}\tan\delta(\theta)d\theta & :DE'\ Section\\ \int_{r'_0}^{r}\frac{dr}{r}=\int_{\theta_0}^{\theta}\tan\delta(\theta)d\theta & :D'E'\ Section\end{cases} \tag{6}$$

So the expression of the failure surface consists of five parts, namely

$$\begin{cases}r_{AC}(\theta)=r_1\exp\left[-\int_{\theta_1}^{\theta}\tan\kappa(\theta)d\theta\right]\\ r_{CD}(\theta)=r_n\exp[(\theta_n-\theta)\tan\varphi]\\ r_{DE'}(\theta)=r_0\exp\left[-\int_{\theta_0}^{\theta}\tan\delta(\theta)d\theta\right]\\ r_{BD'}(\theta)=r_2\exp[(\theta-\theta_2)\tan\varphi]\\ r_{D'E'}(\theta)=r'_0\exp\left[\int_{\theta_0}^{\theta}\tan\delta(\theta)d\theta\right]\end{cases} \tag{7}$$

where

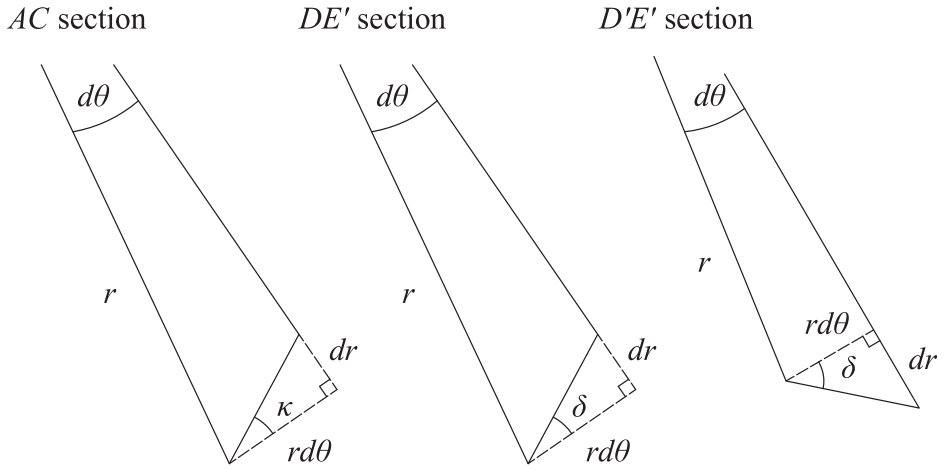

Fig. 3. The infinitesimal elements for *AC*, *DE′* and *D′E′* curves.

$$\begin{cases} r_n = r_1 \exp\left[-\frac{\theta_n-\theta_1}{\kappa_n-\varphi}\ln\frac{\cos\varphi}{\cos\kappa_n}\right] \\ r_0 = r_n\exp[(\theta_n-\theta_0)\tan\varphi] \\ r'_0 = r_2\exp[(\theta_0-\theta_2)\tan\varphi] \end{cases} \tag{8}$$

According to the geometric relationships, r_1, r_2 can be expressed in the form of θ_1, θ_2,

$$\begin{cases} r_1 = \frac{d\sin\theta_2}{\sin(\theta_2-\theta_1)} \\ r_2 = \frac{d\sin\theta_1}{\sin(\theta_2-\theta_1)} \end{cases} \tag{9}$$

Point E' is common to both the curve DE' and $D'E'$, indicating $r_{DE'}(\theta_m) = r_{D'E'}(\theta_m)$. So the relationship between δ_m, θ_0, θ_m can be obtained as follows.

$$\cos\delta_m = \exp\left(\frac{\delta_m-\varphi}{2(\theta_m-\theta_0)}\ln\frac{r_2\exp[(\theta_0-\theta_2)\tan\varphi]}{r_n\exp[(\theta_n-\theta_0)\tan\varphi]}\right)\cos\varphi \tag{10}$$

The infinitesimal element work rate done by gravity of soils can be calculated as

$$dW = \frac{1}{3}\gamma\omega r^3\sin\theta d\theta \tag{11}$$

So the work rate done by gravity of ACC' can be expressed as

$$\begin{aligned} W_{ACC'} &= W_{OAC} - W_{OAC'} \\ &= \tfrac{1}{3}\gamma\omega r_1^3\left\{\int_{\theta_1}^{\theta_n}\exp\left[-3\int_{\theta_1}^{\theta}\tan\kappa(\theta)d\theta\right]\sin\theta d\theta - \frac{\sin^2\theta_1\sin(\theta_n-\theta_1)}{\sin\theta_n}\right\} \\ &= \gamma\omega r_1^3[f_{11}(\theta_1,\theta_n) - f_{12}(\theta_1,\theta_n)] \end{aligned} \tag{12}$$

where $f_{11}(\theta_1,\theta_n)$, $f_{12}(\theta_1,\theta_n)$ can be seen in Appendix.

Similarly,

$$\begin{aligned} W_{CDD'BC'} &= W_{OCD} - W_{OBD'} - W_{OC'B} \\ &= \tfrac{1}{3}\gamma\omega\left\{r_n^3\int_{\theta_n}^{\theta_0}\exp[3(\theta_n-\theta)\tan\varphi]\sin\theta d\theta\right. \\ &\quad \left. - r_2^3\int_{\theta_2}^{\theta_0}\exp[3(\theta-\theta_2)\tan\varphi]\sin\theta d\theta - \frac{r_2^3\sin^2\theta_2\sin(\theta_2-\theta_n)}{\sin\theta_n}\right\} \\ &= \gamma\omega[r_n^3 f_{21}(\theta_n,\theta_0) - r_2^3 f_{22}(\theta_2,\theta_0) - r_2^3 f_{23}(\theta_n,\theta_2)] \end{aligned} \tag{13}$$

where $f_{21}(\theta_n,\theta_0)$, $f_{22}(\theta_2,\theta_0)$, $f_{23}(\theta_n,\theta_2)$ are given in Appendix, and

$$\begin{aligned} W_{DE'D'} &= W_{ODE'} - W_{OD'E'} \\ &= \tfrac{1}{3}\gamma\omega\left\{r_0^3\int_{\theta_0}^{\theta_m}\exp\left[-3\int_{\theta_0}^{\theta}\tan\delta(\theta)d\theta\right]\sin\theta d\theta\right. \\ &\quad \left. - r_0'^3\int_{\theta_0}^{\theta_m}\exp\left[3\int_{\theta_0}^{\theta}\tan\delta(\theta)d\theta\right]\sin\theta d\theta\right\} \\ &= \gamma\omega[r_0^3 f_{31}(\theta_0,\theta_m) - r_0'^3 f_{32}(\theta_0,\theta_m)] \end{aligned} \tag{14}$$

where $f_{31}(\theta_0,\theta_m)$, $f_{32}(\theta_0,\theta_m)$ can be seen in Appendix.

Subsequently, the work rate done by the gravity of the whole failure block W_γ can be written as

$$\begin{aligned} W_\gamma &= W_{ACC'} + W_{CDD'BC'} + W_{DED'} \\ &= \gamma\omega(r_1^3 f_{11} + r_n^3 f_{21} + r_0^3 f_{31} - r_1^3 f_{12} - r_2^3 f_{22} - r_2^3 f_{23} - r_0'^3 f_{32}) \end{aligned} \tag{15}$$

Another part of external work rate is generated by the face pressure provided by a shield machine to retain the tunnel face stability. Supposed that a uniform face pressure σ_T is applied on the tunnel face, its work rate P_σ can be calculated by the following equation.

$$\begin{aligned} P_\sigma &= \int_{\theta_1}^{\theta_2}\sigma_T\frac{r_1\sin\theta_1}{\sin^2\theta}\omega\frac{r_1\sin\theta_1}{\sin\theta}\cos\theta d\theta \\ &= \sigma_T\omega r_1^2 f_{41}(\theta_1,\theta_2) \end{aligned} \tag{16}$$

where $f_{41}(\theta_1,\theta_2)$ can be seen in Appendix.

Based on the assumption of rigid rotation block, the internal energy dissipation is produced along the failure surface. The equation for internal energy dissipation per unit area as given in Eq. (3) is used to calculate the internal work rate by means of integral along AC, DE' and $D'E'$, resulting in

$$\begin{aligned} P_{AC} &= \int_{\theta_1}^{\theta_n} c\omega r_1^2\exp\left[-2\int_{\theta_1}^{\theta}\tan\kappa(\theta)d\theta\right]\left(\cos\varphi\frac{1-\sin\kappa(\theta)}{1-\sin\varphi}\right. \\ &\quad \left. + 2\xi\frac{\sin\kappa(\theta)-\sin\varphi}{\cos\varphi}\right)\frac{1}{\cos\kappa(\theta)}d\theta \\ &= c\omega r_1^2 f_{51}(\theta_1,\theta_n) \end{aligned} \tag{17}$$

$$\begin{aligned} P_{DE'} &= \int_{\theta_0}^{\theta_m} c\omega r_0^2\exp\left[-2\int_{\theta_0}^{\theta}\tan\delta(\theta)d\theta\right]\left(\cos\varphi\frac{1-\sin\delta(\theta)}{1-\sin\varphi}\right. \\ &\quad \left. + 2\xi\frac{\sin\delta(\theta)-\sin\varphi}{\cos\varphi}\right)\frac{1}{\cos\delta(\theta)}d\theta \\ &= c\omega r_0^2 f_{52}(\theta_0,\theta_m) \end{aligned} \tag{18}$$

And

$$\begin{aligned} P_{D'E'} &= \int_{\theta_0}^{\theta_m} c\omega r_0'^2\exp\left[2\int_{\theta_0}^{\theta}\tan\delta(\theta)d\theta\right]\left(\cos\varphi\frac{1-\sin\delta(\theta)}{1-\sin\varphi}\right. \\ &\quad \left. + 2\xi\frac{\sin\delta(\theta)-\sin\varphi}{\cos\varphi}\right)\frac{1}{\cos\delta(\theta)}d\theta \\ &= c\omega r_0'^2 f_{53}(\theta_0,\theta_m) \end{aligned} \tag{19}$$

where $f_{51}(\theta_1,\theta_n)$, $f_{52}(\theta_0,\theta_m)$, $f_{53}(\theta_0,\theta_m)$ are given in Appendix.

The section CD and BD' are log-spiral curves. The internal energy dissipation rate along them can be easily obtained using the following equations.

$$\begin{aligned} P_{CD} &= \int_{\theta_n}^{\theta_0} c\omega r_n^2\exp[2(\theta_n-\theta)\tan\varphi]d\theta \\ &= c\omega r_n^2 f_{54}(\theta_n,\theta_0) \end{aligned} \tag{20}$$

$$\begin{aligned} P_{BD'} &= \int_{\theta_2}^{\theta_0} c\omega r_2^2\exp[2(\theta-\theta_2)\tan\varphi]d\theta \\ &= c\omega r_2^2 f_{55}(\theta_2,\theta_0) \end{aligned} \tag{21}$$

where $f_{54}(\theta_n,\theta_0)$, $f_{55}(\theta_2,\theta_0)$ are given in Appendix.

So the total internal work rate P_d can be calculated by summing the internal energy dissipation rate along AC, DE', $D'E'$, CD and BD' together, that is

$$\begin{aligned} P_d &= P_{AC} + P_{DE'} + P_{D'E'} + P_{CD} + P_{BD'} \\ &= c\omega(r_1^2 f_{51} + r_0^2 f_{52} + r_0'^2 f_{53} + r_n^2 f_{54} + r_2^2 f_{55}) \end{aligned} \tag{22}$$

By making use of the upper bound theorem of limit analysis, the face pressure can be calculated for the proposed failure mechanism as follows.

$$\sigma_T = \frac{\begin{array}{c}\gamma(r_1^3 f_{11} + r_n^3 f_{21} + r_0^3 f_{31} - r_1^3 f_{12} - r_2^3 f_{22} - r_2^3 f_{23} - r_0'^3 f_{32}) \\ - c(r_1^2 f_{51} + r_0^2 f_{52} + r_0'^2 f_{53} + r_n^2 f_{54} + r_2^2 f_{55})\end{array}}{r_1^2 f_{41}} \tag{23}$$

There are seven parameters defining the failure mechanism in Fig. 2, namely θ_1, θ_2, θ_n, κ_n, θ_0, θ_m, δ_m. However, δ_m, θ_0, θ_m are not independent parameters but have a relationship as shown in Eq. (10). So only the first six parameters will be sought by the optimization program for the maximum value of face pressure in Eq. (23), namely the critical face pressure. The ranges of the independent parameters are given in Eq. (24).

$$\begin{cases} 0 < \theta_1 < \pi/2 \\ \theta_1 < \theta_2 < \pi/2 \\ 0 \leqslant \theta_n \leqslant \theta_2 \\ \varphi \leqslant \kappa_n \leqslant \pi/2 \\ \theta_2 < \theta_m < \pi \\ \theta_2 \leqslant \theta_0 < \theta_m \end{cases} \tag{24}$$

where θ_1 and θ_2 determine the overall shape of the failure block while θ_n, θ_0 and θ_m define the portion of the failure mechanism subjected to tensile stress. It can be inferred from Eq. (24) that the section of the failure mechanism governed by the nonlinear strength envelope are searched along the whole failure surface.

Table 1
Numerical results with the variation of c or φ.

c/kPa	φ/°	ξ	θ_1/°	θ_2/°	θ_0/°	θ_m/°	δ_m/°	σ_T/kPa	σ_{T0}/kPa	Difference
10	15	0	14.57	44.57	116.57	125.27	52.50	83.30	81.00	2.8%
15	15	0	14.57	44.57	110.57	121.57	52.50	67.32	62.34	8.0%
20	15	0	14.57	44.57	100.57	115.57	52.50	52.24	43.68	19.6%
25	15	0	14.57	46.57	94.57	113.57	52.50	38.09	25.02	52.2%
30	15	0	14.57	46.57	84.57	107.57	52.50	24.88	6.36	291.2%
20	5	0	18.57	30.57	128.57	136.97	47.50	215.25	178.57	20.5%
20	10	0	14.57	36.57	118.57	132.57	50.00	94.91	79.32	19.7%
20	15	0	14.57	44.57	100.57	115.57	52.50	52.24	43.68	19.6%
20	20	0	14.57	50.57	86.57	102.27	55.00	30.88	25.26	22.2%
20	25	0	16.57	50.57	66.57	81.17	57.50	18.77	14.42	30.2%

4. Parametric analysis and comparison

4.1. Numerical results

Based on the proposed approach, an efficient procedure is written to calculate the critical face pressure of a tunnel in Mohr-Coulomb soils with tensile strength cut-off. Numerical results show that θ_n and κ_n are very close to θ_1 and φ respectively, which means that only the top of the failure block is affected by tensile strength cut-off. Table 1 presents the numerical results of critical face pressures with c ranging from 10 kPa to 30 kPa and φ ranging from 5° to 25°, in which only the full tensile strength cut-off is considered. The unit weight of soils γ is set to 20kN/m^3. The six independent parameters defining the failure mechanism are output as a part of the solutions in Table 1. σ_{T0} denotes the critical face pressure without tensile strength cut-off. The differences between σ_T and σ_{T0} are given in the last column of Table 1.

According to Table 1, either c or φ can affect the parameters of θ_0 and θ_m which respectively define the start and end of the failure block subjected to tensile stress, but the effect of φ is more remarkable. It is of interest to find that the difference between θ_0 and θ_m increases with the increase of c, but remains about 15° with the variation of φ. This phenomenon indicates that the increase of c probably enlarges the area of the failure block subjected to tensile stress. δ_m, the maximum dilatancy angle of soils, is only influenced by the variation of φ. A bigger value of φ results in a bigger value of δ_m which eventually forms a failure block with a gentle corner at the top. This is a more practical failure shape of tunnel face that is probably observed in engineering in comparison with the conventional failure mechanism with a sharp corner. As a matter of fact, what we are most concerned about is the effect of tensile strength cut-off on the critical face pressure which is an important indicator for engineering design. Obviously, the influence of tensile strength cut-off is significant. More specifically, the increase of c or φ makes the influence of tensile strength cut-off more significant. As c changes from 10 kPa to 30 kPa, the relative increment of critical face pressure induced by tensile strength cut-off grows from 2.8% to 291.1%, but it only varies around 20% to 30% with φ ranging from 5° to 25°. So it can be speculated that the influence of tensile strength cut-off is more prominent for hard soils or heavily fractured rock masses which has a relatively big cohesion.

According to the numerical results listed in Table 1, Fig. 4 shows the profiles of tunnel face failure considering the effect of tensile strength cut-off. It can be observed from Fig. 4a that the variation of c has little effect on the failure block in compressive region, but shows a significant influence on the portion of the failure block in tensile regime. From Fig. 4b, we can know that the failure block is greatly affected by the variation of φ. However, it seems to have less contribution to the enlargement of the failure block in tensile regime. The studies on the profile of failure block can give an insight of tunnel face failure with tensile strength cut-off and further verify the correctness of the proposed approach.

As plotted in Fig. 5, the critical face pressures obtained by the

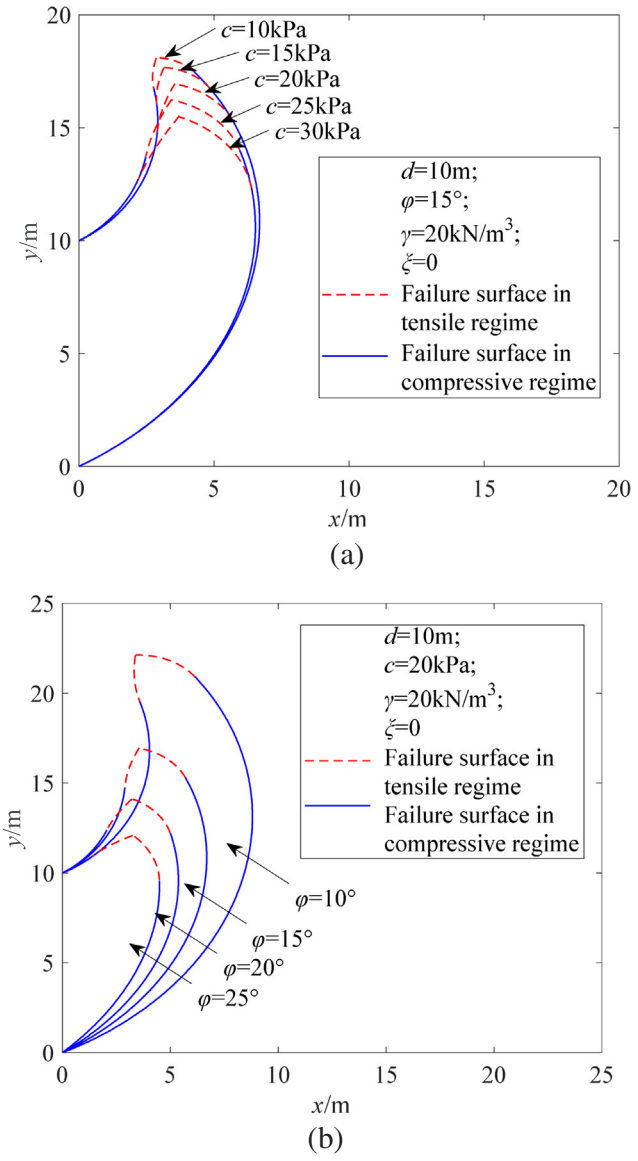

Fig. 4. The profiles of tunnel face failure with tensile strength cut-off (a) with the variation of c (b) with the variation of φ.

proposed approach are compared with those given by conventional rotational failure mechanism without tensile strength cut-off. The absolute difference between the two methods increases with the increase of c while decreases with the increase of φ. The difference reaches the maximum value of 76.84 kPa which corresponds to the case of c = 30 kPa and φ = 5°. The maximum relative difference comes from the case of c = 30 kPa and φ = 15°, arriving at 291.2%. Probably, a

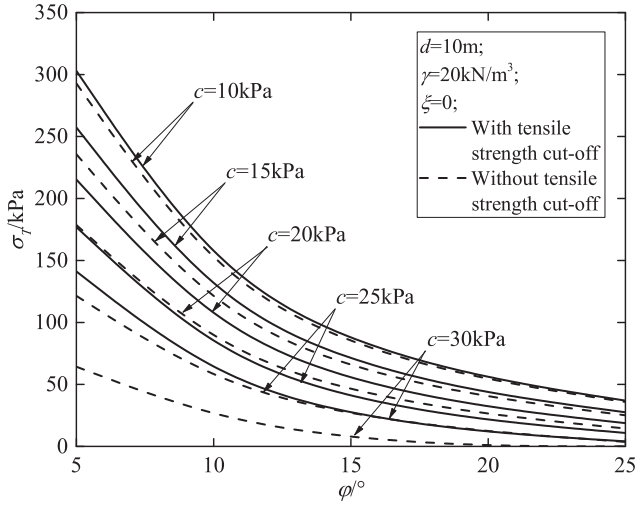

Fig. 5. The comparison of the critical face pressures with and without tensile strength cut-off.

bigger difference can be observed in the case of c = 30 kPa and 20° or c = 30 kPa and φ = 25° because the tunnel face is stable according to the conventional method, but not for the proposed approach.

In order to investigate the influence of γ and ξ on the critical face pressure, the cases of γ = 18 kN/m^3, 20 kN/m^3, 22 kN/m^3 and ξ = 0, 1 are investigated respectively. The numerical results are plotted in Fig. 6. It is shown that the variation of ξ only has a little influence on the critical face pressure and the influence becomes negligible when c or φ is very small. The strategy to deal with tension cut-off in numerical modelling represented by Line 1 in Fig. 1b is also adopted for comparison. As shown in Fig. 6b, its estimated critical support pressure is just between those with ξ = 0 and ξ = 1, which is consistent with its role of the partial tension cut-off. In addition, the increase of γ leads to an increase of the critical face pressure, and it seems that the influence of γ is independent from c or φ.

4.2. Comparison with numerical simulation approach

In this section, the proposed approach is compared with the finite difference method of FLAC3D. The plane strain model of tunnel face is built with a diameter of 10 m and a buried-depth of 20 m as shown in Fig. 7. The unit weight of soils takes 20kN/m^3 in keeping with the previous content. Four cases with different combinations of c and φ are investigated by the numerical simulation approach, including Case 1: c = 10 kPa, φ = 15°; Case 2: c = 20 kPa, φ = 10°; Case 3: c = 20 kPa, φ = 15°; Case 4: c = 20 kPa, φ = 25°. The obtained critical support pressure are compared with those given by the proposed approach as shown in Table 2. Results show that the difference between two methods is around 5% or less for each case which shows the availability of the proposed approach. Fig. 8 presents the contours of maximum shear strain rate in soils when the tunnel face is brought to limit state. It can be seen that the affected zone leans forward when the internal friction angle is small, such as Fig. 8b, which is just consistent with the conclusions from Fig. 4b.

5. Elementary energy analysis

In order to further discuss how the tensile strength cut-off affects the critical face pressure of a tunnel, the elementary energy analysis, mainly referring to the work rate done by gravity E_1 and internal energy dissipation rate E_2, is performed by cutting the rotation angle θ into numerous infinitesimal elements. As shown in Fig. 9, the elementary work rate done by gravity and internal energy dissipation are calculated along the whole failure block. Both the proposed approach and the

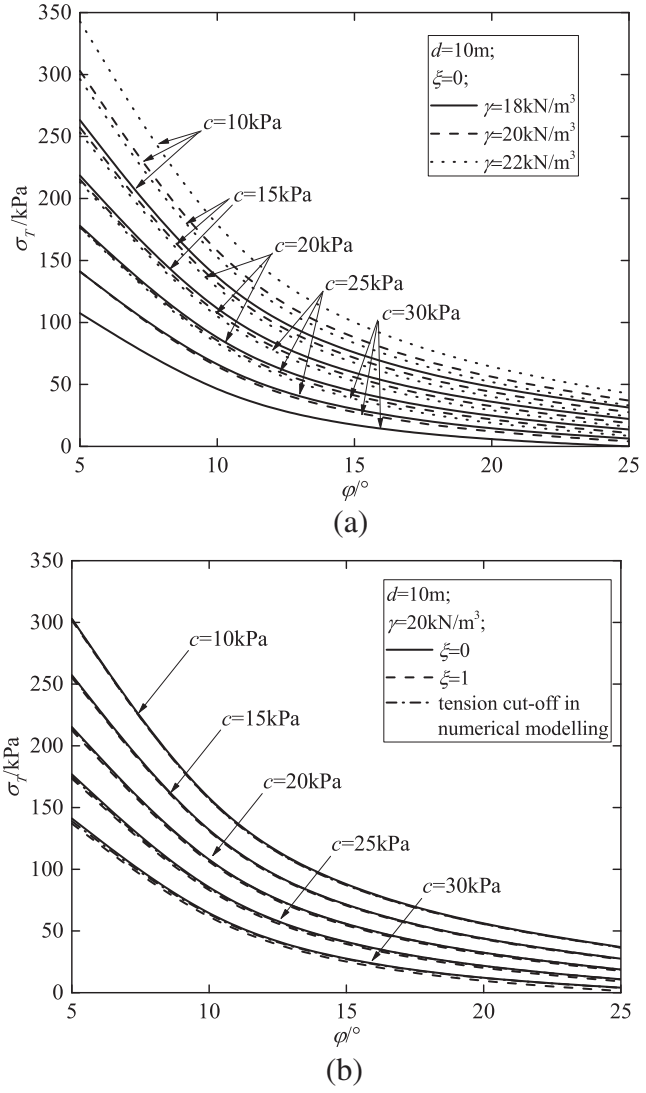

Fig. 6. The influence of γ and ξ on critical face pressures with tensile strength cut-off (a) the variation of γ (b) the variation of ξ.

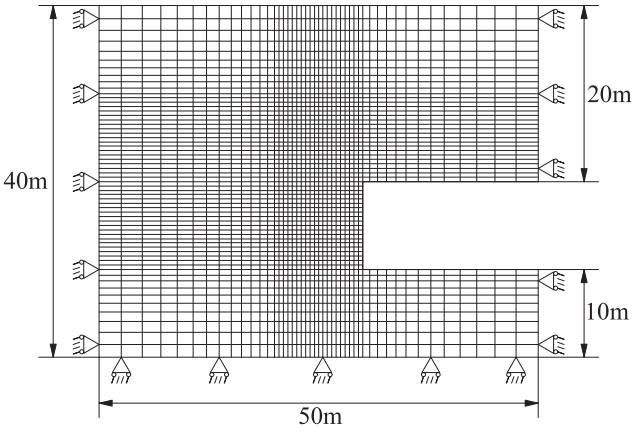

Fig. 7. The numerical model of FLAC3D.

conventional method without tensile strength cut-off are adopted to fulfill this demand. Notice that θ changes from θ_1 to θ_m for the proposed approach and from θ_1 to θ_3 for the conventional method where θ_3 can be calculated by the following equation.

Table 2
Comparison with numerical simulation approach.

No.	Critical support pressure/kPa		Difference
	FLAC3D	The proposed approach	
Case 1	87.10	83.30	4.26%
Case 2	100.40	94.91	5.47%
Case 3	55.30	52.24	5.53%
Case 4	19.20	18.77	2.24%

$$\theta_3 = \frac{1}{2}\left[(\theta_1 + \theta_2) - \frac{\ln(\sin\theta_1/\sin\theta_2)}{\tan\varphi}\right] \tag{25}$$

In addition, the energy dissipation is only produced along the lower boundary of the failure surface when θ ranges from θ_1 to θ_2.

Two case of $c = 10$ kPa, $\varphi = 15^\circ$ and $c = 20$ kPa, $\varphi = 25^\circ$ are considered in this section with the optimization parameters listed in Table 1. According to the critical face pressures given in Table 1, the former case stands for an unstable tunnel face and the latter for a stable one. The results of the elementary energy analysis are presented in Fig. 10. It is shown that $E_1 < E_2$ can be observed for the top of the failure block as well as a small portion at the tunnel invert according to the conventional method. It means that the portion of the failure block will not collapse if it is free from the influence of other portions. This phenomenon becomes more significant for a stable tunnel face. It is of interest to find that the top portion of the failure block satisfying $E_1 < E_2$ is almost eliminated due to the tensile strength cut-off, which is the reason why the required face pressure with tensile strength cut-off becomes bigger. For the proposed approach, the two part of work rate are nearly equal at the point of $\theta = \theta_m$ which is just the end of the failure block with tensile strength cut-off. From this perspective, the modification of tensile strength cut-off to the conventional failure mechanism probably can be explained as that the top of the failure mechanism that satisfies the condition of $E_1 < E_2$ is cut away. This practice allows us to find a more dangerous sliding surface that may occur ahead of tunnel face than any one determined by the classical Mohr-Coulomb yield condition. By comparing Fig. 10a with Fig. 10b, we can see that a bigger value of c or φ will lead to a bigger range that are affected by tensile strength cut-off. The affected region is about from 116° to 123° for the unstable case while from 66° to 79° for the stable case. In addition, the internal energy dissipation rate is more seriously affected than the work rate done by gravity. To put it bluntly,

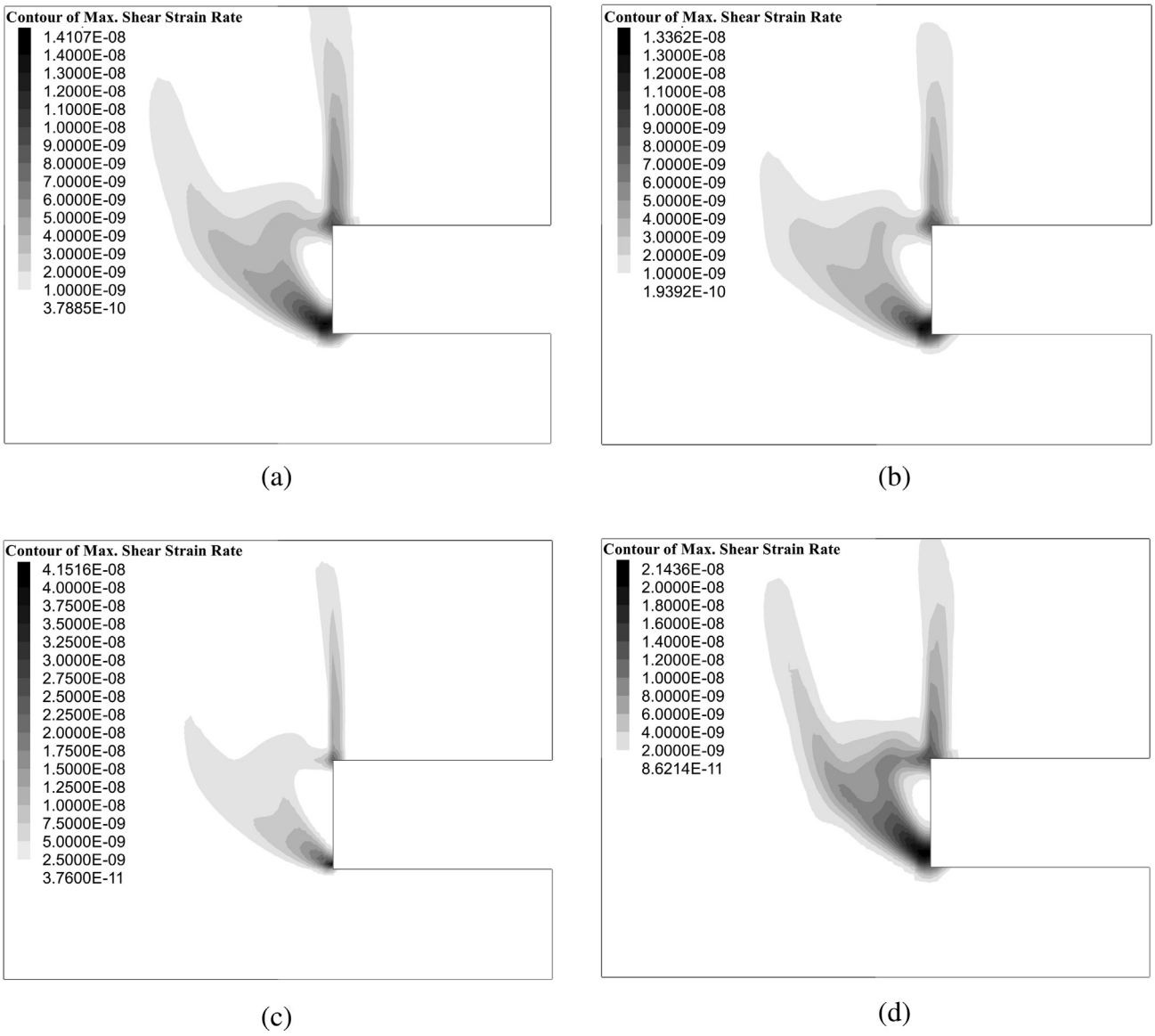

Fig. 8. The contour of maximum shear strain rate of tunnel face (a) Case 1 (b) Case 2 (c) Case 3 (d) Case 4.

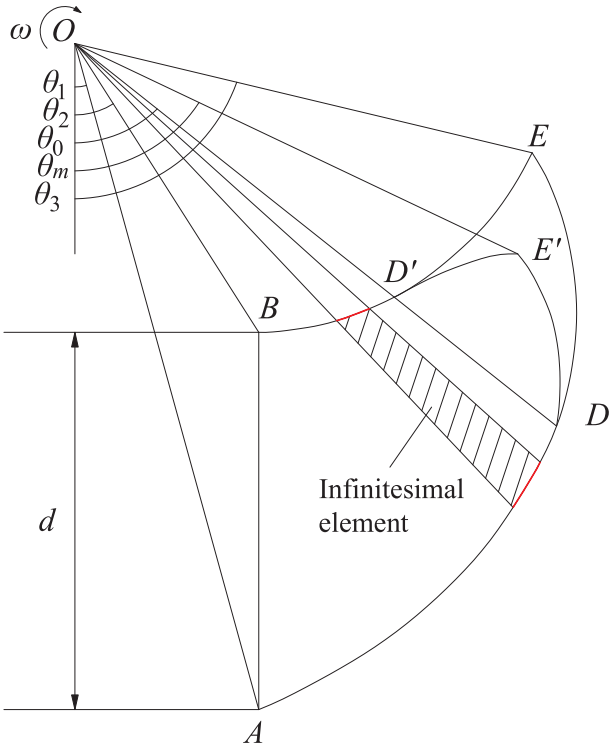

Fig. 9. The schematic diagram for elementary energy analysis of face failure.

the portion of the failure block that satisfies $E_1 < E_2$ plays a role of anti-sliding. So its reduction caused by tensile strength cut-off helps to obtain the most critical face pressure against face failure.

6. Conclusions

In the classical Mohr-Coulomb failure criterion, the strength envelope of geomaterials in tensile regime are extrapolated from the experiment-based strength envelope in compressive regime. In reality, the uniaxial tensile strength of soils is usually very small or even zero which eventually results in a nonlinear strength envelope when the normal stress is close to 0 or tensile stress. So it is essential to consider a reduced or zero tensile strength of soils in stability assessment of tunnel face. This paper presents a modification to the conventional rotational failure mechanism of tunnel face driven in soils considering the effect of tensile strength cut-off. A plane strain model is adopted to fulfill this demand. It allows a nonlinear strength envelope in the tensile regime of Mohr-Coulomb yield condition. A novel procedure is written based on the proposed approach to compute the critical face pressure against tunnel face. Parametric analysis is performed to further discuss the effect of tensile strength cut-off on the critical face pressure. The following conclusions can be drawn.

The portion of the failure block subjected to tensile stress is searched along the whole failure block which shows that the most critical face pressure can be obtained when the tensile stress only appears at the top portion. As a result, a gentle corner is formed at the top of the failure block due to the existence of tensile strength cut-off.

Either c or φ has influences on the failure mechanism of tunnel face with tensile strength cut-off. Comparisons with conventional method indicate that with a range of c from 10 kPa to 30 kPa, the relative increment of critical face pressure induced by tensile strength cut-off grows from 2.8% to 291.1%, but it only varies around 20% to 30% with φ ranging from 5° to 25°. So it is implied that the effect of tensile strength cut-off is more serious in geomaterials with a bigger cohesion. In addition, the maximum dilatancy angle of soils governed by nonlinear strength envelope δ_m depends more on φ than c. The variations of

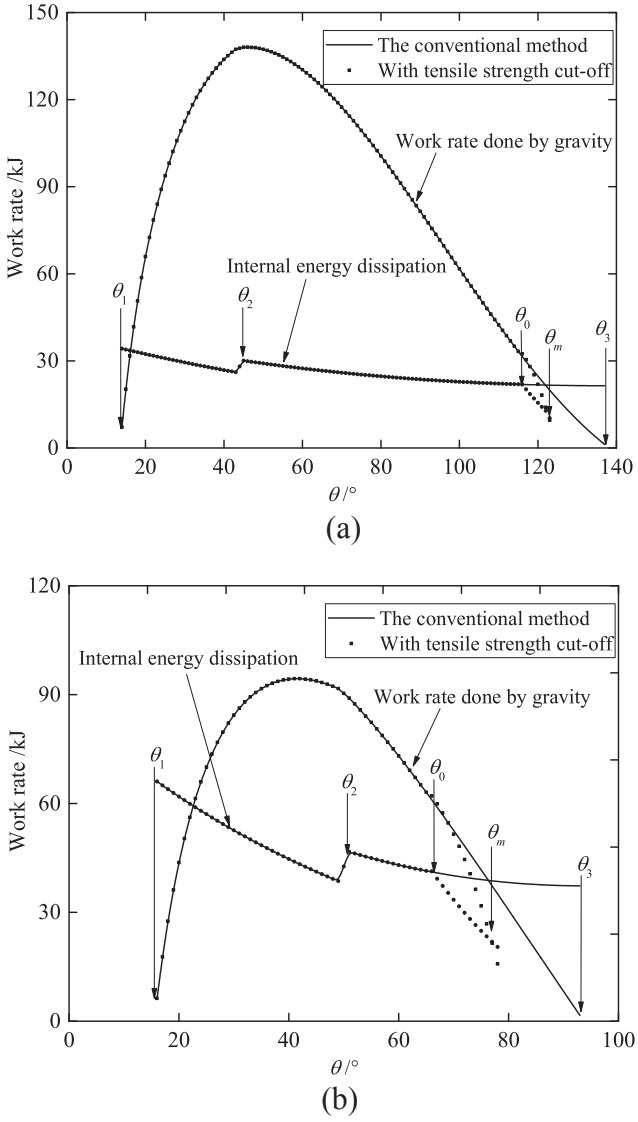

Fig. 10. The elementary energy analysis along the failure surface (a) $c = 10$ kPa, $\varphi = 15°$ (b) $c = 20$ kPa, $\varphi = 25°$.

the unit weight of soils γ and the coefficient ξ are also taken into account. The former shows a significant influence on the critical face pressure while the latter shows a slight influence.

To give a further discussion about the effect of tensile strength cut-off on critical face pressure of a tunnel, the elementary energy analysis is performed by calculating the work rate done by gravity E_1 and internal energy dissipation rate E_2 for each infinitesimal element. Results given by the conventional method show that $E_1 < E_2$ can be observed for the top of the failure block as well as a small portion at the tunnel invert. However, the top portion of the failure block that satisfies $E_1 < E_2$ is almost eliminated due to the tensile strength cut-off. From this perspective, the modification of tensile strength cut-off to the conventional failure mechanism probably can be explained as that the top of the failure mechanism that satisfies the condition of $E_1 < E_2$ is cut away. This practice results in a more dangerous sliding surface of tunnel face and subsequently yields a more critical face pressure.

The innovation of this paper lies in the proposal of an improved rotational failure mechanism of tunnel face in Mohr-Coulomb soils with tensile strength cut-off. Unlike the previously published works, the presented procedure does not limit the soils in tensile regime to the top of the failure zone, but numerically determines which part is affected by tensile stress. An elementary energy analysis is performed to give an

insight of the influence of tensile strength cut-off on tunnel face stability.

Acknowledgement

This study was financially supported by the NSFC (51378510). This funding is greatly appreciated.

Appendix. Failure mechanism of tunnel face with tensile strength cut-off

$$f_{11}(\theta_1, \theta_n) = \frac{1}{3}\int_{\theta_1}^{\theta_n} \exp\left[-\frac{3(\theta_n - \theta_1)}{\kappa_n - \varphi}\ln\frac{\cos\kappa(\theta)}{\cos\kappa_n}\right]\sin\theta d\theta \tag{A1}$$

$$f_{12}(\theta_1, \theta_n) = \frac{\sin^2\theta_1\sin(\theta_n - \theta_1)}{3\sin\theta_n}$$

$$f_{21}(\theta_n, \theta_0) = \frac{3\tan\varphi\sin\theta_n + \cos\theta_n - (3\tan\varphi\sin\theta_0 + \cos\theta_0)\exp[3(\theta_n - \theta_0)\tan\varphi]}{3(1 + 9\tan^2\varphi)} \tag{A2}$$

$$f_{22}(\theta_2, \theta_0) = \frac{(3\tan\varphi\sin\theta_0 - \cos\theta_0)\exp[3(\theta_0 - \theta_2)\tan\varphi] - 3\tan\varphi\sin\theta_2 + \cos\theta_2}{3(1 + 9\tan^2\varphi)} \tag{A3}$$

$$f_{23}(\theta_n, \theta_2) = \frac{\sin^2\theta_2\cdot\sin(\theta_2 - \theta_n)}{3\sin\theta_n} \tag{A4}$$

$$f_{31}(\theta_0, \theta_m) = \frac{1}{3}\int_{\theta_0}^{\theta_m} \exp\left\{\frac{3(\theta_m - \theta_0)}{\delta_m - \varphi}\ln\frac{\cos\delta(\theta)}{\cos\varphi}\right\}\sin\theta d\theta \tag{A5}$$

$$f_{32}(\theta_0, \theta_m) = \frac{1}{3}\int_{\theta_0}^{\theta_m} \exp\left\{-\frac{3(\theta_m - \theta_0)}{\delta_m - \varphi}\ln\frac{\cos\delta(\theta)}{\cos\varphi}\right\}\sin\theta d\theta \tag{A6}$$

$$f_{41}(\theta_1, \theta_2) = \frac{1}{2}\left(1 - \frac{\sin^2\theta_1}{\sin^2\theta_2}\right) \tag{A7}$$

$$f_{51}(\theta_1, \theta_n) = \int_{\theta_1}^{\theta_n} \exp\left\{-\frac{2(\theta_n - \theta_1)}{\kappa_n - \varphi}\ln\frac{\cos\kappa(\theta)}{\cos\kappa_n}\right\}\left(\cos\varphi\frac{1 - \sin\kappa(\theta)}{1 - \sin\varphi} + 2\xi\frac{\sin\kappa(\theta) - \sin\varphi}{\cos\varphi}\right)\frac{1}{\cos\kappa(\theta)}d\theta \tag{A8}$$

$$f_{52}(\theta_0, \theta_m) = \int_{\theta_0}^{\theta_m} \exp\left\{\frac{2(\theta_m - \theta_0)}{\delta_m - \varphi}\ln\frac{\cos\delta(\theta)}{\cos\varphi}\right\}\left(\cos\varphi\frac{1 - \sin\delta(\theta)}{1 - \sin\varphi} + 2\xi\frac{\sin\delta(\theta) - \sin\varphi}{\cos\varphi}\right)\frac{1}{\cos\delta(\theta)}d\theta \tag{A9}$$

$$f_{53}(\theta_0, \theta_m) = \int_{\theta_0}^{\theta_m} \exp\left\{-\frac{2(\theta_m - \theta_0)}{\delta_m - \varphi}\ln\frac{\cos\delta(\theta)}{\cos\varphi}\right\}\left(\cos\varphi\frac{1 - \sin\delta(\theta)}{1 - \sin\varphi} + 2\xi\frac{\sin\delta(\theta) - \sin\varphi}{\cos\varphi}\right)\frac{1}{\cos\delta(\theta)}d\theta \tag{A10}$$

$$f_{54}(\theta_n, \theta_0) = \frac{1 - \exp[2(\theta_n - \theta_0)\tan\varphi]}{2\tan\varphi} \tag{A11}$$

$$f_{55}(\theta_2, \theta_0) = \frac{\exp[2(\theta_0 - \theta_2)\tan\varphi] - 1}{2\tan\varphi} \tag{A12}$$

References

Augarde, C.E., Lyamin, A.V., Sloan, S.W., 2003. Stability of an undrained plane strain heading revisited. Comput. Geotech. 30 (5), 419–430.
Chen, W.F., 1975. Limit Analysis and Soil Plasticity. Elsevier, Amsterdam, the Netherlands.
Dias, D., Kastner, R., 2013. Movements caused by the excavation of tunnels using face pressurized shields analysis of monitoring and numerical modeling results. Eng. Geol. 152 (1), 17–25.
Drucker, D.C., Prager, W., 1952. Soil mechanics and plastic analysis or limit design. Q. Appl. Math. 10 (2), 157–165.
Duncan, J.M., Wright, S.G., 2005. Soil Strength and Slope Stability. John Wiley and Sons Inc, Hoboken, N.J.
Fraldi, M., Guarracino, F., 2011. Evaluation of impending collapse in circular tunnels by analytical and numerical approaches. Tunn. Undergr. Space Technol. 26 (4), 507–516.
Ibrahim, E., Soubra, A.H., Mollon, G., Raphael, W., Dias, D., Reda, A., 2015. Three-dimensional face stability analysis of pressurized tunnels driven in a multilayered purely frictional medium. Tunn. Undergr. Space Technol. 49, 18–34.
Huang, F., Zhang, M., Wang, F., Ling, T.H., Yang, X.L., 2020.. The failure mechanism of surrounding rock around an existing shield tunnel induced by an adjacent excavation. Comput. Geotech. 117, 103236.
Keawsawasvong, S., Ukritchon, B., 2017. Undrained stability of an active planar trapdoor in non-homogeneous clays with a linear increase of strength with depth. Comput. Geotech. 81, 284–293.
Leca, E., Dormieux, L., 1990. Upper and lower bound solutions for the face stability of shallow circular tunnels in frictional material. Geotechnique 40 (4), 581–606.
Li, T.Z., Yang, X.L., 2019. Face stability analysis of rock tunnels under water table using Hoek-Brown failure criterion. Geomech. Eng. 18 (3), 235–245.
Michalowski, R.L., 2017. Stability of intact slopes with tensile strength cut-off. Géotechnique 67 (8), 720–727.
Michalowski, R.L., Drescher, A., 2009. Three-dimensional stability of slopes and excavations. Géotechnique 59 (10), 839–850.
Mollon, G., Dias, D., Soubra, A.H., 2009. Probabilistic analysis and design of circular tunnels against face stability. Int. J. Geomech. 9 (6), 237–249.
Mollon, G., Dias, D., Soubra, A.H., 2011. Rotational failure mechanisms for the face stability analysis of tunnels driven by a pressurized shield. Int. J. Numer. Anal. Meth. Geomech. 35 (12), 1363–1388.
Pan, Q.J., Dias, D., 2017. Upper-bound analysis on the face stability of a non-circular tunnel. Tunn. Undergr. Space Technol. 62, 96–102.
Pan, Q.J., Dias, D., 2018. Three dimensional face stability of a tunnel in weak rock masses subjected to seepage forces. Tunn. Undergr. Space Technol. 71, 555–566.
Park, D., Michalowski, R.L., 2017. Three-dimensional stability analysis of slopes in hard soil/soft rock with tensile strength cut-off. Eng. Geol. 229, 73–84.
Paul, B., 1961. A modification of the Coulomb-Mohr theory of fracture. J. Appl. Mech. 28 (2), 259–268.
Senent, S., Mollon, G., Jimenez, R., 2013. Tunnel face stability in heavily fractured rock masses that follow the Hoek-Brown failure criterion. Int. J. Rock Mech. Min. Sci. 60, 440–451.
Smith, J.V., 2015. A new approach to kinematic analysis of stress-induced structural slope instability. Eng. Geol. 187, 56–59.

Soubra, A.H., 1999. Upper-bound solutions for bearing capacity of foundations. J. Geotech. Geoenviron. Eng. 125 (1), 59–68.
Ukritchon, B., Keawsawasvong, S., 2017. Design equations for undrained stability of opening in underground walls. Tunn. Undergr. Space Technol. 70, 214–220.
Ukritchon, B., Yingchaloenkitkhajorn, K., Keawsawasvong, S., 2017a. Three-dimensional undrained tunnel face stability in clay with a linearly increasing shear strength with depth. Comput. Geotech. 88, 146–151.
Ukritchon, B., Keawsawasvong, S., Yingchaloenkitkhajorn, K., 2017b. Undrained face stability of tunnels in Bangkok subsoils. Int. J. Geotech. Eng. 11 (3), 262–277.
Ukritchon, B., Keawsawasvong, S., 2019a. Lower bound stability analysis of plane strain headings in Hoek-Brown rock masses. Tunn. Undergr. Space Technol. 84, 99–112.
Ukritchon, B., Keawsawasvong, S., 2019b. Lower bound solutions for undrained face stability of plane strain tunnel headings in anisotropic and non-homogeneous clays. Comput. Geotech. 112, 204–217.
Ukritchon, B., Keawsawasvong, S., 2019c. Undrained Stability of Unlined Square Tunnels in Clays with Linearly Increasing Anisotropic Shear Strength. Geotech. Geol. Eng. 1–19.
Yang, X.L., Zhang, S., 2019. Seismic active earth pressure for soils with tension cracks. Int. J. Geomech. 19 (6), 06019009.
Zhang, F., Gao, Y., Wu, Y., Zhang, N., Ukritchon, B., Yingchaloenkitkhajorn, K., Keawsawasvong, S., 2019a. Upper-bound solutions for face stability of circular tunnels in undrained clays. Géotechnique 69 (7), 655–658.
Zhang, D.B., Jiang, Y., Yang, X.L., 2019b. Estimation of 3D active earth pressure under nonlinear strength condition. Geomech. Eng. 17 (6), 515–525.
Zhang, R., Yang, X.L., 2019. New 3D failure analysis of water-filled karst cave beneath deep tunnel. Geomech. Eng. 18 (1), 1–9.
Zingg, S., Anagnostou, G., 2018. Effects of the hydraulic capacity of advance drainage boreholes on tunnel face stability. Tunn. Undergr. Space Technol. 71, 518–530.